



Rosin-derived porous microspheres with robust selective cationic dye adsorption

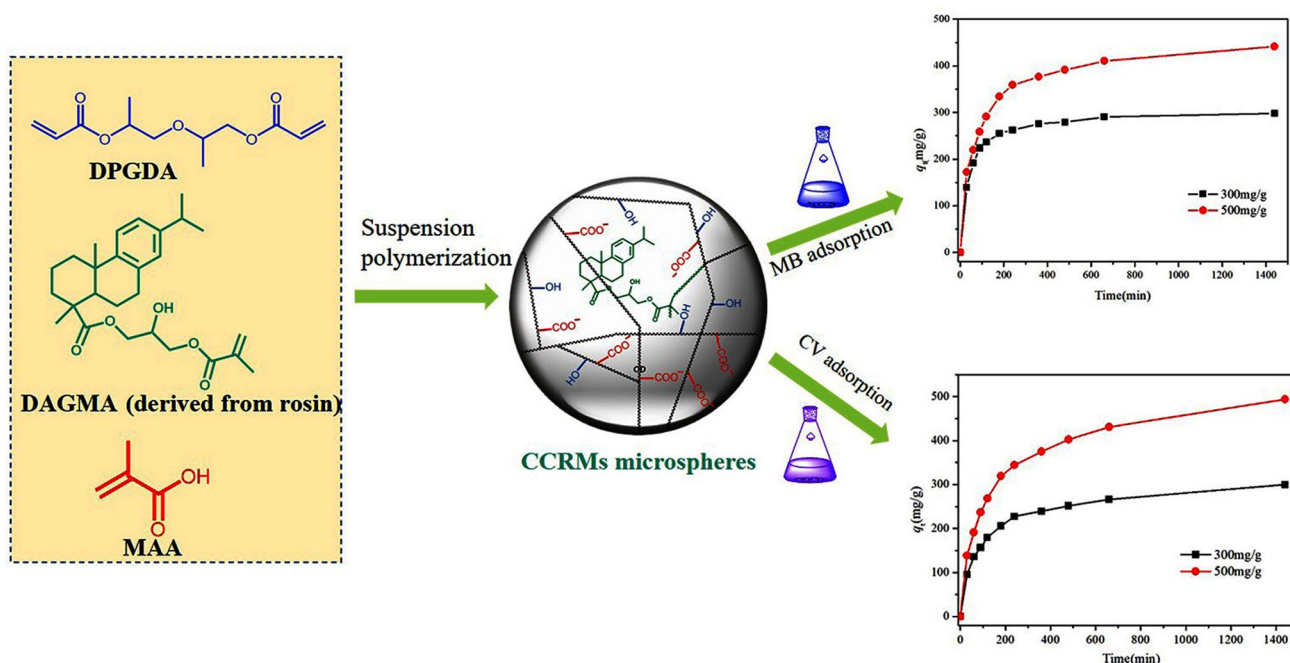
Zenghui Cheng^{1,2,3,4,5} · Chunpeng Wang^{1,2,3,4,5} · Juan Yu⁵ · Meihong Liu^{1,2,3,4,5} · Jifu Wang^{1,2,3,4,5} · Daihui Zhang^{1,2,3,4,5} · Fuxiang Chu^{1,2,3,4,5}

Received: 30 March 2021 / Accepted: 19 May 2021 / Published online: 12 July 2021
© Iran Polymer and Petrochemical Institute 2021

Abstract

The utilization of rosin to fabricate functional polymers has attracted great attention due to its unique structure and property. Herein, we prepared a new type of carboxyl-containing cross-linked rosin microspheres (CCRMs) using a renewable-resource rosin as the raw material through the suspension polymerization. For comparative purpose, vanillin methacrylate (VMA), styrene (St) and isobornyl methacrylate (IBOMA) were separately used to replace DAGMA as monomer for the preparation of microspheres. Our results indicated that the obtained porous CCRMs showed a broad size distribution ranging from mesopores (3–50 nm) to macropores (> 50 nm), whereas the counterparts derived from VMA, St or IBOMA showed a powder state. Moreover, the CCRMs exhibited moderately high thermal stability. The integration of DAGMA into polymer microspheres provided CCRMs with excellent adsorption ability, which exhibited robust selective cationic dye (e.g., methylene blue (MB) and crystal violet (CV)) adsorption from waste aqueous solution. The adsorption process was fitted well with the Langmuir isotherm and the pseudo-second-order kinetic model. The maximum adsorption capacity was observed to be 602.4 mg/g for CV at 40 °C, and 512.8 mg/g for MB at 20 °C. In general, the high dye adsorption properties suggest that CCRMs may be highly efficient in adsorption selectivity for some cationic dyes.

Graphic abstract



Keywords Adsorption · Dyes · Methylene blue · Crystal violet · Rosin · Polymer microspheres

Introduction

Using renewable feedstock to prepare polymeric materials is receiving tremendous attention from both academic and industrial fields because of their potential in replacing or partially replacing the petroleum-based materials. Rosin is a kind of natural resin produced from pine trees. The annual production of rosin was estimated more than 1 million metrics [1]. Resin acid (around 85%) bearing a bulky hydrophobic hydrophenanthrene structure, is the main component of rosin, which has been reported to be extensively used for adhesives tackifiers, coating, soaps, varnishes and so forth.

Recently, rosin has been reported to be used as a renewable feedstock for manufacture of polymeric materials [2] by free radical polymerization [3], click chemistry [4], ring-opening polymerization [5, 6], condensation polymerization [7], etc. Ganewatta and coworkers reported a surface-initiated atom transfer radical polymerization (ATRP) strategy toward surface-immobilized rosin acid-derived cationic homopolymer using a novel rosin-derived acrylate monomer as feedstock. This homopolymer-grafted substrate exhibited strong antimicrobial activity against bacteria [8]. Liu and coworkers [9] adapted the “grafting from” ATRP for the preparation of two series of rosin-based graft copolymers. Cheng et al. [10] reported a series of grafted copolymers from rosin, fatty acid and ethyl cellulose by a “grafting from” reversible addition-fragmentation chain transfer polymerization (RAFT) of DAGMA (derived from rosin) and LMA (derived from fatty acid). The intrinsic rigidity and acidity derived from rosin acid could give the polymer integrity with excellent mechanical properties, chemical stability and other performance advantages.

Dyes are extensively used in textile, paper-making, color photography, leather, food, printing and plastic industries for coloring [11]. However, these industries produce large amounts of dye-containing wastewater that is difficult to biodegrade in aqueous solution, leading to toxicity to humans and the environment [12]. Methylene blue (MB) and crystal violet (CV) are two common cationic dyes consisting of various aromatic amine groups, which are reported to be highly carcinogenic and mutagenic. As a result, various physical, chemical and biological methods, such as coagulation, biological oxidation, membrane filtration, biological oxidation, etc., have been developed for the removal of MB and CV from wastewaters to reduce their negative impact on the environment [13, 14].

Since most dyes have abundant aromatic rings, much effort has been devoted to develop the adsorption material containing the benzene ring, which is considered to be the dye adsorbent. It is reported that the benzene ring

contributed the π - π stacking interactions existing between the adsorbent and adsorbate. In view of the aromatic rings in rosin acid, rosin was reported to fabricate adsorption material for removal of phenolic compounds [15], metal ions [16, 17], bisphenol A [18], basic orange II [19], MB [20] and malachite green dye [21], etc. For example, Li and coworkers [22] converted rosin into ethylene glycol maleic rosinate acrylate that was used as a cross-linker to fabricate the rosin-based polymer microspheres (RBPMs) through suspension polymerization. RBPMs could be used as a polymeric adsorption material for concentrating coptidis total alkaloids and purifying berberine hydrochloride (BBH) from the coptidis rhizoma extracts. However, the reports on rosin-based polymers used for the adsorption of dyes (particularly for the adsorption of MB and CV) are rare.

Herein, we report a suspension polymerization strategy to synthesize a new type of carboxyl-containing cross-linked rosin-based microspheres (CCRM) that is used for the adsorption of MB and CV from wasted water. Then, the adsorption performance of CCRM was evaluated by detail investigation on the influence of different dyes, solution pH, contact time, contact temperature, and initial dye concentration on the MB or CV adsorption.

Experimental

Materials

2-Methacryloyloxyisopropanol ester of dehydroabiatic acid (DAGMA) was prepared according to our previous work [23]. Dipropylene glycol diacrylate (DPGDA, > 80% (GC)), vanillin methacrylate (VMA), styrene (St), isobornyl methacrylate (IBOMA), benzoyl peroxide (BPO, AR), congo red (CR, > 98%), crystal violet (CV, 98%) and methylacrylic acid (MAA, AR, > 99.0%) were all purchased from Aladdin Chemistry Co. Ltd. (Shanghai, China), and used as received. Polyvinyl pyrrolidone (PVP, K30) and sodium dodecyl sulfate (SDS) were purchased from Sinopharm Chemical Reagent Co. Ltd. Rhodamine B (RhB, $\geq 99.0\%$) was purchased from Shanghai Macklin Biochemical Co. Ltd. Hydrochloric acid (HCl), ethyl acetate and 1-octane were purchased from Nanjing Chemical Reagent Co. Ltd. Methylene blue (MB, $\geq 98.5\%$), acid orange 74 (AO) and methyl orange (MO) were all analytical grades and provided by Tianjin Chemical Reagent Research Institute.

Characterization

The FTIR spectra (ATR) were recorded using a Nicolet iS50-spectrometer. Thermogravimetric analysis (TGA) was performed on a NETZSCH TG209F1 thermogravimetric analyzer from room temperature to 800 °C at a heating rate of 10 °C/min under nitrogen. Scanning electron microscopy (SEM) was performed with a S3400N electron microscope (Hitachi) working at 15 kV acceleration voltage. Brunauer–Emmett–Teller (BET) was carried out in an ASAP2020M adsorption apparatus (Micromeritics Instruments Corporation) at 77 K. An ultraviolet–visible spectrophotometer (UV–Vis, UV-1800PC, Shanghai MAPADA) was used.

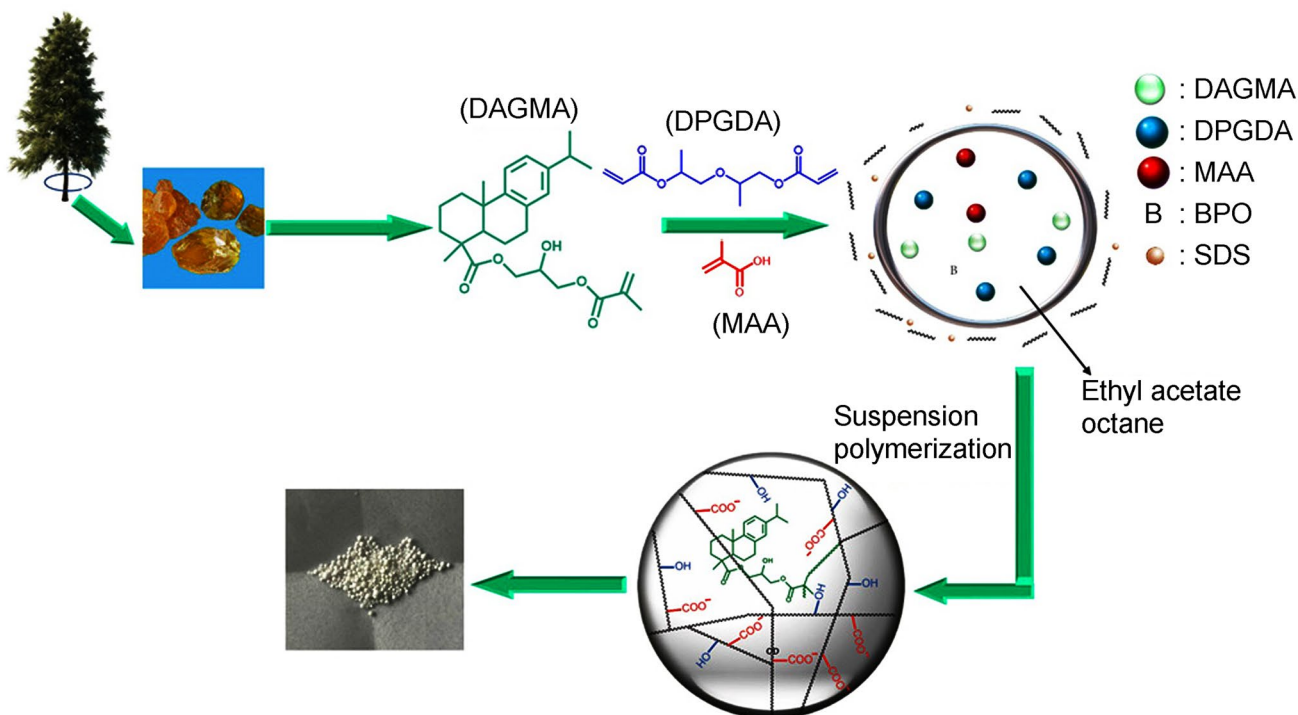
Preparation of CCRMs

Suspension polymerization strategy was applied to synthesize CCRMs according to the previous report [24] (Scheme 1). First, we prepared the oil phase by mixing DAGMA (1.0 g) or other monomer, MAA (0.5 g), BPO (0.1 g) and the cross-linker DPGDA (3.0 g) with a solvent mixture (22.5 mL) composed of ethyl acetate and 1-octane (volume ratio = 2/1). Meanwhile, PVP (1% by wt) and SDS (0.04% by wt) aqueous solutions were charged in a flask to form an aqueous phase. Subsequently, the aqueous phase was vigorously stirred at a rate of 400 r/min for 10 min,

and the oil phase was dropped into the flask with a constant stirring (600 r/min) within 30 min at room temperature. The reaction was carried out at 90 °C for 2 h. The polymer particles were formed, followed by the extraction with ethanol and deionized water for 30 h to remove unreacted monomers and other substances. A 10% NaOH solution was used to treat the polymer particles and to ionize the –COOH groups in the microspheres to –COO[−] groups. Finally, deionized water was applied to wash the microspheres until the liquid was neutral. The obtained CCRMs were dried for further use. For comparative purpose, VMA, St and IBOMA were also used to prepare microspheres with the same procedure, respectively.

Adsorption studies

Adsorption behavior of CCRMs for dyes was investigated in batches. The method used for this study is described as follows: 20 mg of the microspheres and 20 mL of an aqueous of dye were charged in a 50 mL Erlenmeyer flask. The flask was oscillated at a speed of 150 r/min until reaching equilibrium. The dyes residual solution concentration was recorded with UV–Vis at the corresponding maximum absorption wavelengths at 590, 663, 478, 462 and 494 nm for CV, MB, AO, MO and CR, respectively. Equation (1) was used to calculate the adsorption capacity, q_e (mg/g) at the equilibrium time (h):



Scheme 1 A general strategy for CCRMs derived from rosin

$$q_e = \frac{V(c_0 - c_e)}{m} \quad (1)$$

where q_e is the adsorption capacity at equilibrium (mg/g), c_0 and c_e represent the initial and equilibrium concentrations (mg/L), respectively, m is the mass of adsorbent (g) and V represents the volume of the dye solution (L).

The effect of pH by mixing 20 mg of CCRMs microspheres into 20 mL dye solutions was studied. The pH values were set from 2.0 to 10.0 at 30 °C in 500 mg/L MB solution or 600 mg/L CV solution. pH of the solution was adjusted by dilute HCl or NaOH aqueous solutions.

To study the adsorption isotherms, 20 mg of CCRMs microspheres were added into 20 mL dye solutions with different initial MB and CV concentrations varied from 50 to 1000 mg/L at three temperatures (20, 30 and 40 °C) for 24 h.

Kinetic experiments were performed by varying initial dye concentrations (300, 500 mg/L) at 30 °C with adding 20 mg CCRMs microspheres. The concentration of dye solution after adsorption at predefined time intervals was analyzed. The adsorption capacity at time t (min) was calculated by the following equation:

$$q_t = \frac{V(c_0 - c_t)}{m} \quad (2)$$

where c_0 (mg/L) is the initial concentrations, c_t is the concentration at time t (mg/L), V is the volume of the dye solution (L) and m is the mass of adsorbent (g).

Results and discussion

Characterization of polymer microspheres

We employed suspension polymerization to prepare the carboxyl-containing cross-linked rosin microspheres (CCRMs) using DAGMA as a monomer, DPGDA as a cross-linking agent, MAA as a functional monomer and BPO as an initiator. For comparative purpose, VMA, St and IBOMA were separately used to replace DAGMA as monomer for the preparation of microspheres. The SEM images were applied to study the morphologies of microspheres. Figures 1 and S1 (in supplementary material) illustrate the morphologies of different cross-linked microspheres synthesized from different monomers with the same polymerization process. CCRMs exhibit a regular spheres morphology and the numerous pores distributed on the surface of microspheres, whereas the counterpart derived from VMA, St or IBOMA showed a status of powder. Specially, CCRMs have large particle sizes (greater than 100 μm) and the larger pores. Moreover, the internal structure of microspheres appear rough with porous cavities, which can display more active site in the absorption process. Therefore, the as-synthesized CCRMs were supposed to have a great potential as a good adsorbent for removing organic dyes from polluted water.

The CCRMs were then characterized by FTIR. As shown in Fig. 2, the disappearance of the adsorption peak at 1637 cm⁻¹ (–C(CH₃)=C) in CCRMs presented the successful polymerization of DAGMA through suspension polymerization. The adsorption peaks at 1450 cm⁻¹ were attributed to the stretching vibration of aromatic ring carbon skeleton. The peak at 752 cm⁻¹ was assigned to the stretching vibrations of C–H and CH=CH₂ in the aromatic ring. The characteristic peaks at 1379 cm⁻¹ corresponded

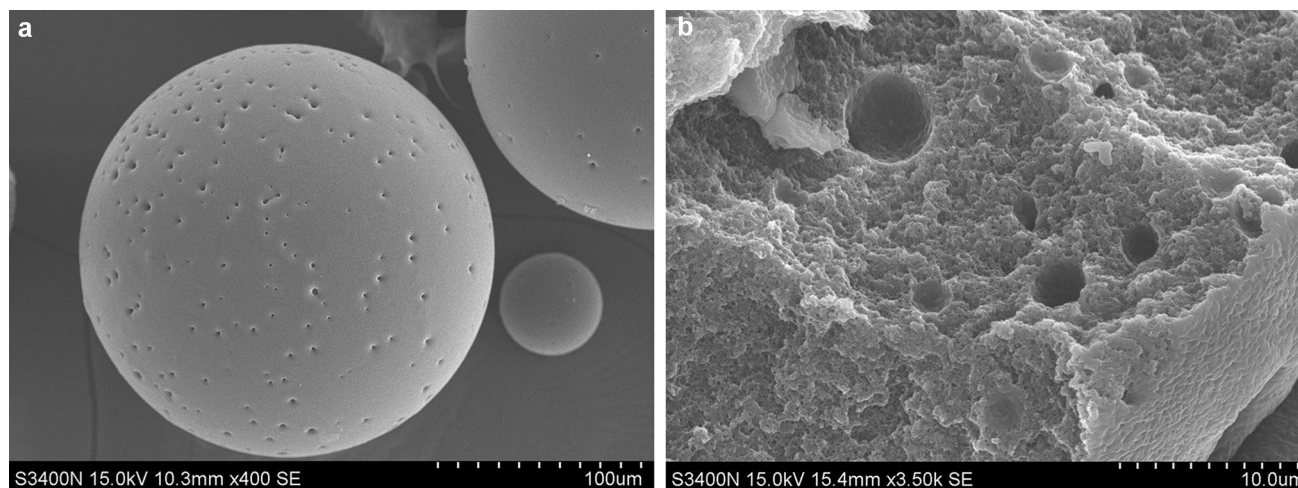


Fig. 1 SEM images of CCRMs

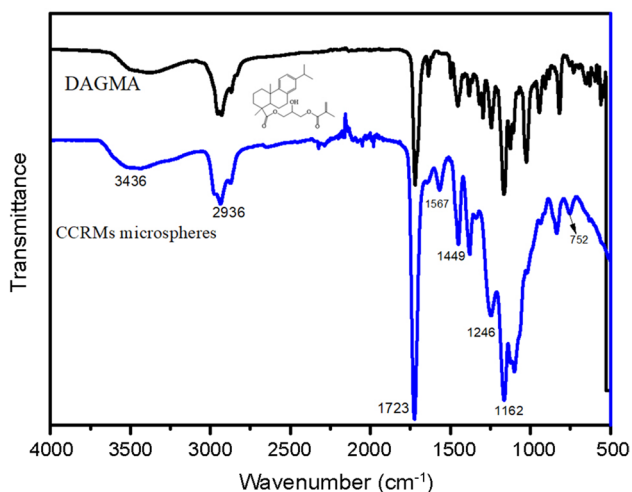


Fig. 2 FTIR spectra of DAGMA monomer and CCRMs

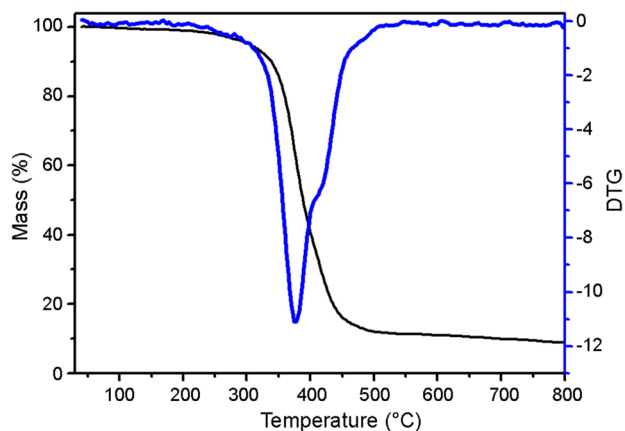


Fig. 3 TGA and DTG thermograms of CCRMs

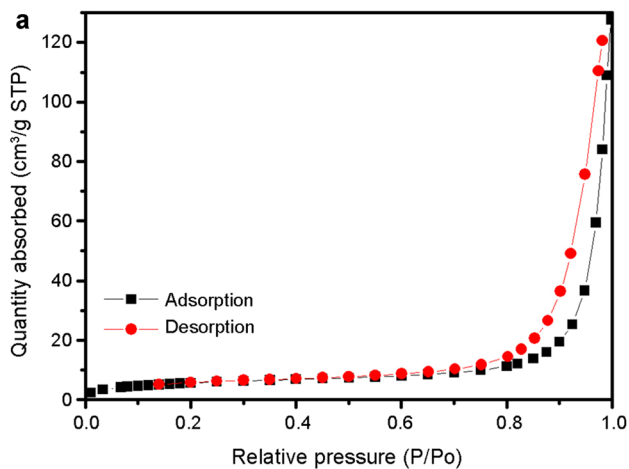


Fig. 4 Nitrogen adsorption–desorption isotherm obtained at 77 K for the CCRMs

to in-plane bending of O–H. These results confirmed that DAGMA was introduced into the polymer microspheres. In addition, the adsorption peak at 3436 cm^{-1} resembled the characteristic stretching vibration of -OH in CCRMs. The adsorption peak at 1723 cm^{-1} was assigned to the stretching vibration of C = O bond. The peak observed at around 1162 cm^{-1} was attributed to the bending vibration of C–O bond, while the peak at around 1567 cm^{-1} was assigned to carboxyl groups [25]. Based on these results, the attachment of various functional groups on the CCRMs surface was verified.

The thermal stability and degradation behavior of CCRMs were evaluated by TGA. As shown in Fig. 3, CCRMs exhibited a one-stage decomposition. CCRMs were initially decomposed from 341.1 °C and ended at 480 °C , indicating that CCRMs have a moderately high thermal stability.

The specific surface area and average pore size of the CCRMs were investigated by BET with typical N_2 adsorption–desorption isotherms (Fig. 4). According to the standard BET method, the specific surface area of CCRMs was measured to be about $20.82\text{ m}^2/\text{g}$, which is larger than that of some other microspheres [26, 27]. The isotherms of the CCRMs exhibited typical type-II behavior with a hysteresis loop in the relative pressure range of 0.7–1.0, implying the presence of pore structures in the CCRMs. Furthermore, the pore diameter showed a broad size distribution ranging from mesopores (3–50 nm) to macropores (> 50 nm), which was consistent with the results of SEM.

Adsorption performance

Adsorption capacity of CCRMs for different dyes

To verify the adsorption characteristics of CCRMs, three different microspheres originated from VMA, St or IBOMA were also used to adsorb MB in parallel. The results are summarized in Fig. S2 (in supplementary material). It was found that CCRMs have the highest adsorption capacity. This could be explained by π - π stacking interactions existing between MB molecules and the three-ring phenanthrene skeleton structure of the rosin in CCRMs [28].

For further evaluation of the adsorption property of CCRMs, we carried out its adsorption test on the anionic dyes (e.g., AO, MO, CR) and cationic dyes (e.g., RhB, CV, MB), respectively. The concentration of dyes was uniformly controlled at 500 mg/L and the temperature was set at 30 °C. The adsorption results are shown in Fig. 5. It was found that CCRMs exhibited higher adsorption for MB and CV with an equilibrium adsorption capacity of 441 and 493 mg/g, respectively. However, the adsorption capacity of MO, AO, CR and RhB was only 0, 12.4, 0 and 128.36 mg/g, respectively. We hypothesized that high selective adsorption property is derived from the three-ring phenanthrene skeleton structure of the rosin in CCRMs, which is likely to enhance π - π stacking interactions existing between MB (or CV) and microspheres. The high selective adsorption property of CCRMs for MB and CV may result from their inherited characters and abundant micropores. In addition, CV and MB are both cationic dyes having amine groups in their structure [29] (Fig. S3, in supplementary material), which could facilitate the adsorption by negatively charged surfaces of CCRMs through the electrostatic interaction with cationic dyes, although RhB is cationic dye having amine group. The space steric hindrance resulted from the lateral chains (long alkyl chains of RhB are close to N^+ centers)

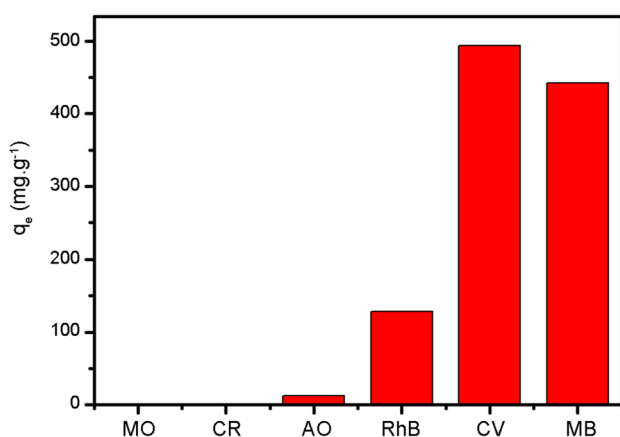


Fig. 5 Adsorption capacities of different dyes on CCRMs

weakened the electrostatic attraction and π - π stacking interactions [27]. These results confirmed our hypothesis. Herein, the adsorption model of CCRMs was established with MB and MV as the target pollutant in the following experiments.

Effect of pH

The pH of an adsorption solution is a decisive factor for adsorption capacity of adsorbent [30]. Therefore, the effect of pH on the adsorption performance of MB (or CV) was evaluated. The dye concentrations were set to 500 mg/L MB solution or 600 mg/L CV solution at 30 °C. Under this concentration condition, all dyes solutions could achieve saturated adsorption based on their adsorption isotherms and the obtained results are presented in Fig. 6. It was found that the adsorption capacity substantially decreased as the pH decreased from 10 to 2. Particularly, the absorbance dropped drastically at pH below 4. This phenomenon is probably due to the presence of high concentration of H^+ ions, which promote the protonation of functional groups. At acidic pH, $-COO^-$ will protonate the cationic to form $-COOH_2^+$. In addition, MB and CV are cationic dyes. As a result, the electrostatic attraction between CCRMs and positively charged cationic dyes have decreased under acidic condition, leading to the restriction of the cationic dye adsorption [31]. A similar trend has been reported for the pH effect on the CV and MB adsorption in the previous reports [32, 33].

Equilibrium isotherm models of dyes

To better understand the surface properties of CCRMs and the adsorption behavior, the adsorption isotherms of MB and CV were established by the initial concentrations varied from 50 to 1000 mg/L at three temperatures of 20, 30 and 40 °C for 24 h. Figure 7a, c shows the effects of initial

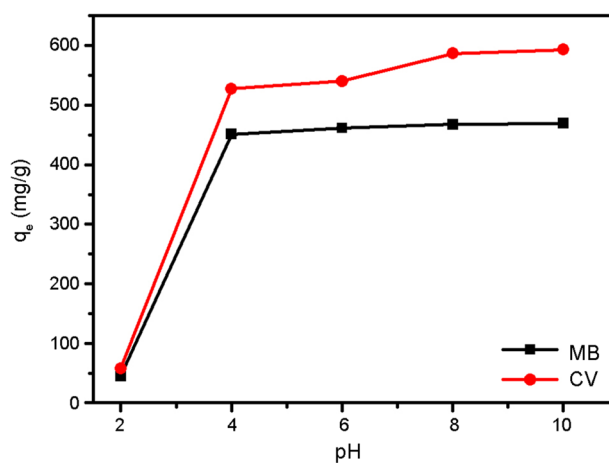


Fig. 6 Effect of pH on MB and CV adsorption

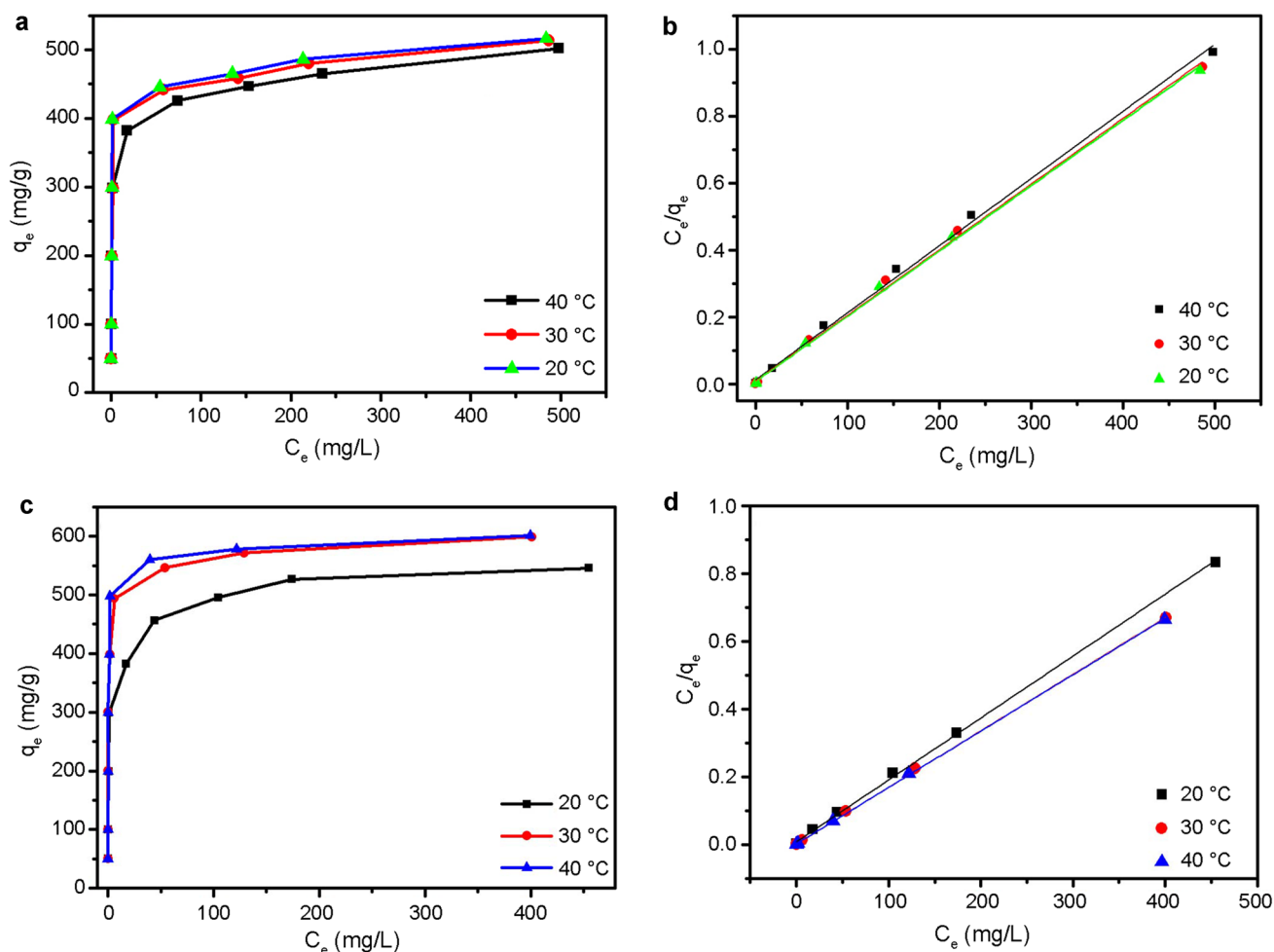


Fig. 7 **a** Adsorption isotherms of MB onto CCRMs. **b** Langmuir isotherm model of MB onto CCRMs. **c** Adsorption isotherms of CV onto CCRMs. **d** Langmuir isotherm model of CV onto CCRMs

concentration and temperature on the MB and CV adsorption capacity of CCRMs. With the increase of initial concentration, the adsorption capacities of two dyes reflect a significant increasing trend. The results indicated that the adsorption process is highly dependent on initial dye concentration, which can be ascribed to the quicker diffusion rate of MB and CV in the higher initial concentration solution, resulting in the higher adsorption capacity.

Different adsorption isotherm models were used to describe the experimental equilibrium data obtained from the study of the absorption of MB and CV. The equations and parameters of Freundlich, Langmuir, Redlich–Peterson and Dubinin–Radushkevich isotherm models are listed in Table S1. They were also applied to examine the experimental data (Fig. 7b, d, and Fig. S4a–f) and the isotherm parameters are summarized in Table 1. It can be clearly observed that the linear correlation coefficients (R^2) of the Langmuir model were higher than those of other models for both dyes, suggesting that the Langmuir isotherm model might be more

suitable to describe the homogeneous adsorption process of MB and CV on CCRMs. Therefore, it can be concluded that MB and CV adsorption on CCRMs may be a monolayer adsorption process.

According to the Langmuir isotherm model, CV theoretical maximum adsorption capacity (q_{max}) was calculated to 602.4 mg/g, which is close to the experimental value. In addition, when the temperature increased from 20 to 40 °C, the q_{max} increased from 546.5 to 598.8 mg/g, indicating that the adsorption process was endothermic. However, it was found that the CCRM adsorption capacity for MB gradually decreased from 512.8 to 497.5 mg/g with increasing temperature, indicating that the adsorption process is exothermic in nature. These results are in agreement with previous reports [29]. A comparison of adsorption capacities of MB and CV on CCRMs with counterparts is shown in Tables S2 and S3. It was found that the maximum q_e values can reach 516.33 and 600.71 mg/g for MB and CV when the initial concentration is 1000 mg/L, which are larger than that of many

Table 1 Fitted isotherm parameters and their goodness of fit to the adsorption data

Dye	$T/^\circ\text{C}$	Langmuir isotherm parameters			Freundlich isotherm parameters		
		q_{max} ($\text{mg}\cdot\text{g}^{-1}$)	K_L ($\text{L}\cdot\text{mg}^{-1}$)	R^2	$K_F(\text{mg}^{1-n}\text{L}^n\text{g}^{-1})$	n	R^2
MB	20	512.8	0.269	0.9985	244.65	7.59	0.7891
	30	510.2	0.232	0.9981	231.42	7.15	0.8130
	40	497.5	0.176	0.9975	208.56	6.57	0.8800
CV	20	546.5	0.221	0.9992	212.15	5.80	0.8691
	30	598.8	0.535	0.9997	281.66	6.90	0.7440
	40	602.4	0.754	0.9998	296.53	7.26	0.6751

Dye	$T/^\circ\text{C}$	Redlich-Peterson				Dubinin–Radushkevich		
		K_{RP}	a_{RP}	g	R^2	q_m ($\text{mg}\cdot\text{g}^{-1}$)	K_{DR}	R^2
MB	20	847.86	1.7596	0.9986	0.9460	475.03	$1.05\cdot 10^{-7}$	0.9450
	30	660.28	1.5316	0.9790	0.9630	452.57	$1.347\cdot 10^{-7}$	0.9100
	40	989.41	2.9360	0.9401	0.9940	430.795	$9.26\cdot 10^{-8}$	0.9051
CV	20	702.67	1.9756	0.9292	0.9650	478.12	$1.57\cdot 10^{-7}$	0.9124
	30	1419.70	2.9631	0.9632	0.8930	532.75	$5.4\cdot 10^{-8}$	0.8654
	40	1193.27	2.1057	0.9930	0.8880	545.93	$5.68\cdot 10^{-8}$	0.8638

Table 2 Thermodynamic parameters for adsorption of MB and CV on CCRMs

Dyes	T ($^\circ\text{C}$)	ΔG° (kJ/mol)	ΔS° ($\text{J}/(\text{mol}\text{K})$)	ΔH° (kJ/mol)
MB	20	-27.68	37.34	-16.81
	30	-28.25		
	40	-28.47		
CV	20	-27.79	260.4	48.66
	30	-30.97		
	40	-32.88		

other previously reported polymeric adsorbents (Table S2). Moreover, comparative study of different rosin-based adsorbents was also carried out and the results are summarized in Table S3. It was found that the synthesized CCRMs showed the higher adsorption capacity.

Thermodynamic of adsorption

The enthalpy change (ΔH°), entropy change (ΔS°) and Gibbs free energy change (ΔG°) as the most important thermodynamic parameters, were employed to describe the adsorption process of the two dyes on CCRMs. As shown in Table 2 and Fig. S5, ΔG° values are all negative (-27.68, -28.25, -28.47 kJ/mol for MB at 20, 30 and 40 $^\circ\text{C}$, and -27.79, -30.97, -32.88 kJ/mol for CV at 20, 30 and 40 $^\circ\text{C}$, respectively). These results confirmed the spontaneous nature and the feasibility of the adsorption [12]. The ΔH° value for the adsorption process of MB on CCRMs is -16.81 kJ/mol, indicating the exothermic nature of the adsorption of MB. The ΔS° was positive, but ΔG° was still negative, suggesting that

the MB adsorption process was mainly driven by the entropy effect [34]. Meanwhile, the positive values of ΔH° revealed that the adsorption of CV dyes on CCRMs was an endothermic process, which is agreed with the effect of temperature. The ΔH° value for the adsorption procedures of CV on CCRMs is 48.66 kJ/mol, indicating that chemisorption dominated the adsorption procedures. The positive ΔS° showed the increased disorder at the solid–solution interface during adsorption, which enhanced the contact opportunities between the dye molecules and CCRMs [35].

Adsorption kinetics

As shown in Fig. 8a, b, the adsorption rate of MB and CV decreased gradually with increasing adsorption time. This can be explained by the adsorption of dye molecules which initially occurred on the outer surface of adsorbent. The dye was then diffused into the internal pores of the adsorbent. Moreover, compared to the lower initial dye concentration, it took longer to achieve equilibrium for higher initial dye concentration.

To further investigate the adsorption process of MB and CV on CCRMs, the experimental data were analyzed using pseudo-first-order (Eq. 3) and pseudo-second-order kinetic models (Eq. 4) [36]:

$$q_t = q_e(1 - e^{-k_1 t}) \quad (3)$$

$$q_t = \frac{k_2 q_e^2 t}{1 + k_2 q_e t} \quad (4)$$

where q_t (mg/g) indicates the adsorption capacity of dyes at time t (min) and q_e (mg/g) presents equilibrium. The

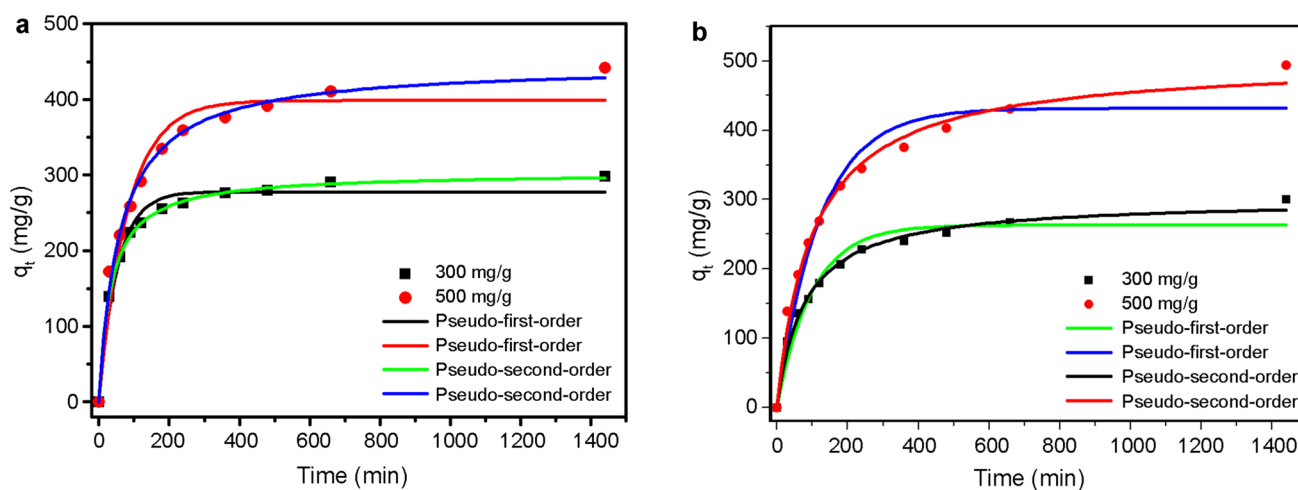


Fig. 8 Non-linear fits of pseudo-first-order and pseudo-second-order kinetic models to (a) MB and (b) MV adsorption at concentrations of 300 and 500 mg/L ($T=30\text{ }^{\circ}\text{C}$)

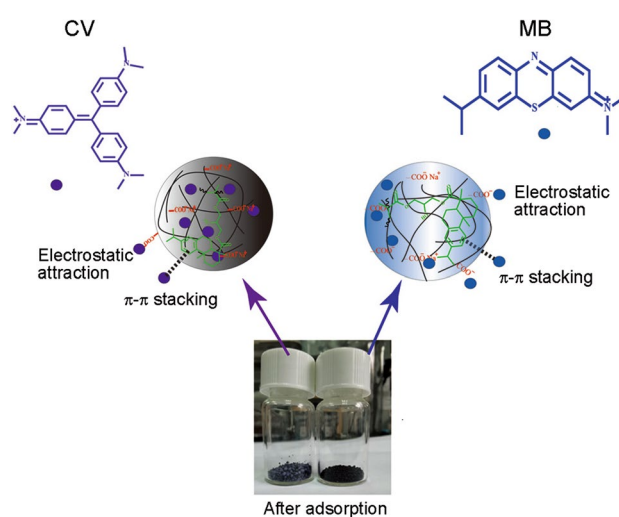
Table 3 Kinetic parameters for adsorption of MB and CV on CCRMs

Dye	Concentrations (mg·L ⁻¹)	Pseudo-first-order			Pseudo-second order			$q_{e,\text{exp}}$ (mg·g ⁻¹)
		q_e (mg·g ⁻¹)	K_1 (min ⁻¹)	R^2	K_2 (g·mg ⁻¹ ·min ⁻¹)	q_e (mg·g ⁻¹)	R^2	
MB	300	277.83	0.019	0.979	$9.58 \cdot 10^{-5}$	303.2	0.999	298.03
	500	398.83	0.012	0.959	$3.73 \cdot 10^{-5}$	446.6	0.993	441.74
CV	300	263.26	0.010	0.954	$4.27 \cdot 10^{-5}$	300.3	0.992	299.79
	500	431.65	0.008	0.951	$1.97 \cdot 10^{-5}$	500.7	0.991	493.72

constants k_1 (min⁻¹) and k_2 (g mg⁻¹ min⁻¹) are the constant rate of pseudo-first order and pseudo-second order, respectively. The adsorption kinetics curves are shown in Fig. 8a, b and the corresponding kinetic parameters of the two models are summarized in Table 3. It was found that the experimental data for both adsorptions of the MB and CV are better consistent with the pseudo-second-order adsorption kinetic models resulting from their better R-squared. Moreover, the experimental value ($q_e = 299.79$ mg/g, 493.72 mg/g) was fitted well with theoretical equilibrium adsorption ($q_e = 300.29$ mg/g, 500.7 mg/g). This result indicated that the adsorption process could be well described by the pseudo-second-order model. Therefore, the chemical adsorption was regarded as the rate-determining step controlling the process of adsorption of MB and CV on CCRMs in terms of the pseudo-second-order kinetic model [37].

Possible adsorption mechanism of the CCRMs

We assumed that the dye molecules were attached on the surface of the adsorbent as a monolayer and were dominated mainly by chemisorption according to adsorption kinetics and isotherm models. Since CV and MB are cationic dyes having amine groups in their structure, they are prone to



Scheme 2 Interactions between the CCRMs, CV and MB

dissociate into Cl^- and dye^+ in aqueous solutions, by which they can interact with the anionic sites on the CCRMs through their cationic nitrogen sites.

As shown in Scheme 2, no significant change in the morphology of CCRMs before and after adsorption of MB

and CV was observed except that the color became a dye color. The FTIR spectra of CCRMs show the change in the adsorption peaks after MB or CV adsorption (Fig. 9). When CV and MB were adsorbed into CCRMs, new adsorption peaks were observed at 1358 and 1328 cm^{-1} , corresponding to -C-N-stretching , and peak at 1122 cm^{-1} was clearly observed that was assigned to $\text{-COO} \leftrightarrow \text{N}$. These results verified the interaction between the protonated nitrogen of the MB, CV and the COO^- of CCRMs. The possible interactions between CCRMs and these two dyes are schematically illustrated in Scheme 2. The π - π stacking interactions also could occur between the aromatic ring of dyes molecule and the aromatic ring of CCRMs [31].

Conclusion

We demonstrated the successful synthesis of several CCRMs porous structures through a convenient and efficient suspension polymerization method. The incorporation of DAGMA into polymer microspheres provided CCRMs with excellent adsorption ability, which is favorable for the isolation of cationic MB and CV dyes from wastewater. The effect of pH on CV and MB adsorption showed that the adsorption of these two dyes is highly dependent on initial solution pH. The adsorption isotherm fitted well to the Langmuir model. The maximum adsorption capacity obtained from the non-linear form of Langmuir isotherm was observed to be 602.4 mg/g for MV at 40 $^{\circ}\text{C}$, and 512.8 mg/g for MB at 20 $^{\circ}\text{C}$. The remarkable adsorption performance can be attributed to the π - π stacking, electrostatic interactions and the structure properties of CCRMs. Kinetic studies confirmed that the adsorption of MB and CV could be described by non-linear form of pseudo-second-order kinetics, suggesting that chemisorption of CV and MB occurs on the CCRMs.

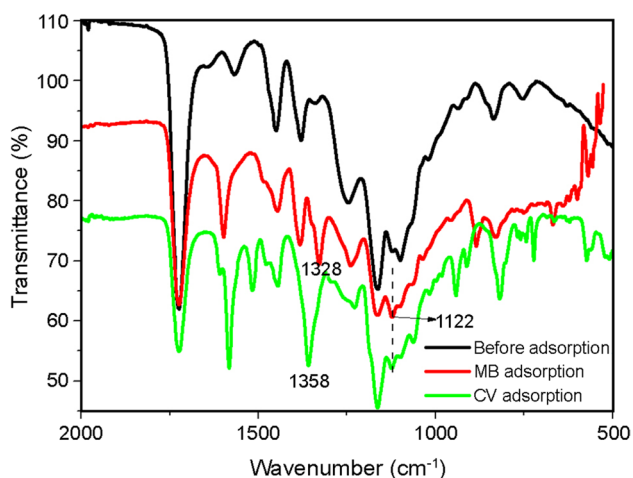


Fig. 9 FTIR spectra of CCRMs, after MB and CV adsorption

These results demonstrated that the CCRMs are new adsorbents, and can be considered as a potential competitor for the removal of cationic dyes in terms of high efficiency, low cost and ecofriendly nature.

Supplementary Information The online version contains supplementary material available at <https://doi.org/10.1007/s13726-021-00955-4>.

Acknowledgements This work was financially supported by the Jiangsu Province Biomass Energy and Materials Laboratory (JSBEM-S-202009), Foundation of National Natural Science Foundation of China (31971600) and National Key Research and Development Program of China (2017YFE0106800).


Author contribution Zenghui Cheng: investigation, designed and writing—original draft; Juan Yu and Meihong Liu: performed experiments; Daihui Zhang: analyzed the data; Chunpeng Wang: resources and methodology; Jifu Wang and Fuxiang Chu: contributed to writing—review and editing.

References

1. Wang J, Liu S, Yu J, Lu C, Wang C, Chu F (2017) Rosin-derived monomers and their progress in polymer application. *Sustain Polym Biomass* 17:103–149
2. Atta AM, Mansour R, Abdou MI, Sayed AM (2004) Epoxy resins from rosin acids: synthesis and characterization. *Polym Adv Technol* 15:514–522
3. Ding W, Wang S, Yao K, Ganewatta MS, Tang C, Robertson ML (2017) Physical behavior of triblock copolymer thermoplastic elastomers containing sustainable rosin-derived polymethacrylate end blocks. *ACS Sustain Chem Eng* 5:11470–11480
4. Yu J, Lu C, Wang C, Wang J, Fan Y, Chu F (2017) Sustainable thermoplastic elastomers derived from cellulose, fatty acid and furfural via ATRP and click chemistry. *Carbohydr Polym* 176:83–90
5. Ganewatta MS, Ding W, Rahman MA, Yuan L, Wang Z, Hamidi N, Robertson ML, Tang C (2016) Biobased plastics and elastomers from renewable rosin via “living” ring-opening metathesis polymerization. *Macromolecules* 49:7155–7164
6. Rahman MA, Lokupitiya HN, Ganewatta MS, Yuan L, Stefik M, Tang C (2017) Designing block copolymer architectures toward tough bioplastics from natural rosin. *Macromolecules* 50:2069–2077
7. Lei YF, Wang XL, Liu BW, Ding XM, Chen L, Wang YZ (2020) Fully bio-based pressure-sensitive adhesives with high adhesivity derived from epoxidized soybean oil and rosin acid. *ACS Sustain Chem Eng* 8:13261–13270
8. Ganewatta MS, Miller KP, Singleton SP, Mehrpouya-Bahrami P, Chen YP, Yan Y, Nagarkatti M, Nagarkatti P, Decho AW, Tang C (2015) Antibacterial and biofilm-disrupting coatings from rosin acid-derived materials. *Biomacromolecules* 16:3336–3344
9. Liu Y, Yao K, Chen X, Wang J, Wang Z, Ploehn HJ, Wang C, Chu F, Tang C (2014) Sustainable thermoplastic elastomers derived from renewable cellulose, rosin and fatty acids. *Polym Chem* 5:3170–3181
10. Cheng Z, Liu Y, Zhang D, Lu C, Wang C, Xu F, Wang J, Chu F (2019) Sustainable elastomers derived from cellulose, rosin and fatty acid by a combination of “graft from” RAFT and isocyanate chemistry. *Int J Biol Macromol* 131:387–395

11. Rafatullah M, Sulaiman O, Hashim R, Ahmad A (2010) Adsorption of methylene blue on low-cost adsorbents: a review. *J Hazard Mater* 177:70–80
12. Yu Y, Qiao N, Wang D, Zhu Q, Fu F, Cao R, Wang R, Liu W, Xu B (2019) Fluffy honeycomb-like activated carbon from popcorn with high surface area and well-developed porosity for ultra-high efficiency adsorption of organic dyes. *Bioresour Technol* 285:121340
13. Lin Q, Gao M, Chang J, Ma H (2016) Adsorption properties of crosslinking carboxymethyl cellulose grafting dimethyldiallylammonium chloride for cationic and anionic dyes. *Carbohydr Polym* 151:283–294
14. You H, Chen J, Yang C, Xu L (2016) Selective removal of cationic dye from aqueous solution by low-cost adsorbent using phytic acid modified wheat straw. *Colloids Surf A Physicochem Eng* 509:91–98
15. Liu S, Wang J, Huang W, Tan X, Dong H, Goodman BA, Du H, Lei F, Diao K (2019) Adsorption of phenolic compounds from water by a novel ethylenediamine rosin-based resin: interaction models and adsorption mechanisms. *Chemosphere* 214:821–829
16. Ruan ZH, Wu JH, Huang JF, Lin ZT, Li YF, Liu YL, Cao PY, Fang YP, Xie J, Jiang GB (2015) Facile preparation of rosin-based biochar coated bentonite for supporting $\alpha\text{-Fe}_2\text{O}_3$ nanoparticles and its application for Cr(vi) adsorption. *J Mater Chem A* 3:4595–4603
17. Tan WX, Lin ZT, Bu HT, Tian Y, Jiang GB (2012) Nano-micelles based on a rosin derivative as potent sorbents and sinking agents with high absorption capabilities for the removal of metal ions. *RSC Adv* 2:7279–7289
18. Yu C, Shan J, Chen Y, Shao J, Zhang F (2020) Preparation and adsorption properties of rosin-based bisphenol A molecularly imprinted microspheres. *Mater Today Commun* 24:101076
19. Li X, Li M, Li J, Lei F, Su X, Liu M, Li P, Tan X (2014) Synthesis and characterization of molecularly imprinted polymers with modified rosin as a cross-linker and selective SPE-HPLC detection of basic orange II in foods. *Anal Methods* 6:6397–6406
20. Wadhwa P, Jindal R, Dogra R (2020) Insight into adsorption kinetics and isotherms for adsorption of methylene blue using gum rosin alcohol/psyllium-based green adsorbent. *Iran Polym J* 29:501–514
21. Kaith BS, Jindal R, Sharma R (2015) Synthesis of a gum rosin alcohol-poly(acrylamide) based adsorbent and its application in removal of malachite green dye from waste water. *RSC Adv* 5:43092–43104
22. Li P, Qin L, Wang T, Dai L, Li H, Jiang J, Zhou J, Li H, Cheng X, Lei F (2020) Preparation and adsorption characteristics of rosin-based polymer microspheres for berberine hydrochloride and separation of total alkaloids from coptidis rhizoma. *Chem Eng J* 392:123707
23. Shaofeng L, Chuanwei L, Chunpeng W, Jifu W, Fuxiang C (2017) Synthesis and characterization of 2-methacryloyloxyisopropanol ester of dehydroabiatic acid. *Chem Ind Forest Prod* 37:89–94
24. Zhang H, Yong X, Zhou J, Deng J, Wu Y (2016) Biomass vanillin-derived polymeric microspheres containing functional aldehyde groups: preparation, characterization, and application as adsorbent. *ACS Appl Mater Interfaces* 8:2753–2763
25. Yan H, Li H, Yang H, Li A, Cheng R (2013) Removal of various cationic dyes from aqueous solutions using a kind of fully biodegradable magnetic composite microsphere. *Chem Eng J* 223:402–411
26. Fu J, Chen Z, Wang M, Liu S, Zhang J, Zhang J, Han R, Xu Q (2015) Adsorption of methylene blue by a high-efficiency adsorbent (polydopamine microspheres): kinetics, isotherm, thermodynamics and mechanism analysis. *Chem Eng J* 259:53–61
27. Fu J, Xin Q, Wu X, Chen Z, Yan Y, Liu S, Wang M, Xu Q (2016) Selective adsorption and separation of organic dyes from aqueous solution on polydopamine microspheres. *J Colloid Interface Sci* 461:292–304
28. Ai L, Zhang C, Liao F, Wang Y, Li M, Meng L, Jiang J (2011) Removal of methylene blue from aqueous solution with magnetite loaded multi-wall carbon nanotube: kinetic, isotherm and mechanism analysis. *J Hazard Mater* 198:282–290
29. Sakin Omer O, Hussein MA, Hussein BHM, Mgaidi A (2018) Adsorption thermodynamics of cationic dyes (methylene blue and crystal violet) to a natural clay mineral from aqueous solution between 293.15 and 323.15 K. *Arab J Chem* 11:615–623
30. Saeed A, Sharif M, Iqbal M (2010) Application potential of grapefruit peel as dye sorbent: kinetics, equilibrium and mechanism of crystal violet adsorption. *J Hazard Mater* 179:564–572
31. Zou J, Liao K, Xiang L, Liu M, Xie F, Liu X, Yu J, An X, Wang Y (2020) Synthesis of poly(cyclotriphosphazene-co-4,4'-diaminodiphenylsulfone) microspheres and their adsorption properties for cationic dyes (methylene blue). *J Inorg Org Polym Mater* 30:976–985
32. Dotto GL, Santos JMN, Rodrigues IL, Rosa R, Pavan FA, Lima EC (2015) Adsorption of methylene blue by ultrasonic surface modified chitin. *J Colloid Interface Sci* 446:133–140
33. Zhang H, Chen L, Li L, Yang Y, Liu X (2017) Magnetic porous carbon microspheres synthesized by simultaneous activation and magnetization for removing methylene blue. *J Porous Mater* 24:341–353
34. Zhao L, Yu B, Xue F, Xie J, Zhang X, Wu R, Wang R, Hu Z, Yang ST, Luo J (2015) Facile hydrothermal preparation of recyclable S-doped graphene sponge for Cu^{2+} adsorption. *J Hazard Mater* 286:449–456
35. Wang B, Zhang Q, Xiong G, Ding F, He Y, Ren B, You L, Fan X, Hardacre C, Sun Y (2019) Bakelite-type anionic microporous organic polymers with high capacity for selective adsorption of cationic dyes from water. *Chem Eng J* 366:404–414
36. Zhuang S, Wang J (2019) Removal of cobalt ion from aqueous solution using magnetic graphene oxide/chitosan composite. *Environ Prog Sustain Energy* 38:S32–S41
37. Saber-Samandari S, Saber-Samandari S, Joneidi-Yekta H, Mohseni M (2017) Adsorption of anionic and cationic dyes from aqueous solution using gelatin-based magnetic nanocomposite beads comprising carboxylic acid functionalized carbon nanotube. *Chem Eng J* 308:1133–1144

Authors and Affiliations

Zenghui Cheng^{1,2,3,4,5} · Chunpeng Wang^{1,2,3,4,5} · Juan Yu⁵ · Meihong Liu^{1,2,3,4,5} · Jifu Wang^{1,2,3,4,5}  · Daihui Zhang^{1,2,3,4,5} · Fuxiang Chu^{1,2,3,4,5}

✉ Jifu Wang
wjf118@126.com

✉ Daihui Zhang
zdh0824@163.com



✉ Fuxiang Chu
chufuxiang@caf.ac.cn

¹ Institute of Chemical Industry of Forest Products, CAF,
Nanjing 210042, Jiangsu Province, China

² National Engineering Laboratory for Biomass Chemical
Utilization, Nanjing 210042, Jiangsu Province, China

³ Key and Open Laboratory of Forest Chemical Engineering,
SFA, Nanjing 210042, Jiangsu Province, China

⁴ Key Laboratory of Biomass Energy and Material,
Nanjing 210042, Jiangsu Province, China

⁵ Co-Innovation Center of Efficient Processing and Utilization
of Forest Resources, Nanjing Forestry University,
Nanjing 210037, China